Magnetism of small supported rhodium particles studied by means of ^{103}Rh nuclear magnetic resonance

2002 J. Phys.: Condens. Matter 14 7135

(http://iopscience.iop.org/0953-8984/14/30/304)

INSTITUTE OF PHYSICS PUBLISHING JOURNAL OF PHYSICS: CONDENSED MATTER

J. Phys.: Condens. Matter **14** (2002) 7135–7145 PII: S0953-8984(02)36425-7

Magnetism of small supported rhodium particles studied by means of ^{103}Rh nuclear magnetic resonance

Séverine Burnet[1], **T Yonezawa**[2] **and J J van der Klink**[1]

[1] Institut de Physique des Nanostructures, Ecole Polytechnique Fédérale de Lausanne, CH-1015 Lausanne, Switzerland
[2] Department of Applied Chemistry, Nagoya University, Nagoya, 464-8603 Japan

E-mail: jacques.vanderklink@epfl.ch

Received 1 May 2002
Published 17 July 2002
Online at stacks.iop.org/JPhysCM/14/7135

Abstract

We present experimental evidence from ^{103}Rh nuclear spin–lattice relaxation rates that small (average diameter 2.6 nm) supported Rh particles show antiferromagnetic susceptibility enhancement at temperatures below 80 K. Slightly larger particles (3.6 nm) have a density of states at the Fermi level on surface sites that is higher than that in the bulk.

1. Introduction

In pure bulk metals, magnetism is found only in the 3d row of the periodic system, from Cr to Ni. Bulk alloys of 'nonmagnetic' elements can be magnetic: $ZrZn_2$ has a Curie temperature of 18 K. Nonbulk forms of 4d and 5d metals can also be magnetic, either due to surface effects as in films [1] or because of size effects, as in atomic clusters [2]. Metallic *para*magnetism can also be modified by surface and size effects. These modifications are often studied using the nuclear magnetic resonance (NMR) technique [3], to avoid the background effects that can be problematic in measurements of the static magnetic susceptibility. Early attempts to detect the paramagnetic quantum size effect [4] have used ^{63}Cu NMR of small copper particles embedded in a matrix [5, 6]. Slichter and co-workers [7] have shown that the particle size dependence of the ^{195}Pt NMR spectrum of small supported platinum particles should be interpreted as a surface effect rather than a size effect. Such systems are models for heterogeneous catalysts, and therefore they have been studied extensively by means of NMR [8].

From the values of Knight shift and relaxation rate of those ^{195}Pt nuclei that are in (or near to) the particle surface, it has been deduced that the local susceptibility in the surface layer is lower than that of the bulk, while the bulk value is retrieved about three atomic layers deep [9]. At least qualitatively, this agrees with calculations for a five-layer platinum film [10]. Bulk palladium has a strongly Stoner-enhanced Pauli susceptibility [11] and is considered a nearly ferromagnetic metal [12], but the calculated local density of states (LDOS) at the Fermi energy on its surfaces is less than in the bulk [13–15]. Like for platinum therefore, the local

susceptibility at the surface of palladium is expected to be less than in the bulk. The calculated Stoner enhancement for bulk rhodium is rather small [11], but the calculated surface LDOS is larger than the bulk value [15, 16]. The experimental situation is not quite clear [17], but suggests that the Rh(100) surface shows superparamagnetism or some extremely unstable two-dimensional ferromagnetic order. In rhodium clusters of up to roughly a hundred atoms, size-dependent magnetism has been found both experimentally [18] and in calculations [15].

The incipient magnetic structure of a paramagnetic system is best described by its wavevector-dependent susceptibility $\tilde{\chi}(\boldsymbol{q})$. In this respect, calculations give distinct results for bulk Pd and bulk Rh [19–21]. The $\tilde{\chi}(\boldsymbol{q})$ of Pd peaks strongly at zero wavevector and decays monotonically for larger $\boldsymbol{q}$, characteristic for an incipient ferromagnet. The calculated $\boldsymbol{q} = \boldsymbol{0}$ enhancement in Rh is clearly weaker than that in Pd; but there is a rather strong secondary maximum that corresponds to a tendency towards antiferromagnetic ordering.

In this paper we use the NMR of ^{103}Rh of small supported rhodium particles to study some of these issues. For large enough particle sizes, there should be mainly 'surface' effects, like in the platinum case. Smaller particles could show magnetic 'size' effects. As a prerequisite for the data analysis, we give a brief review of spin fluctuation theory as applied to NMR and we deduce a number of parameter values from bulk ^{103}Rh NMR data. To mark the peculiarities of Rh, we make occasional comparisons with the properties of Pd.

2. Theory

The theory of the NMR of paramagnetic metals [3, 22] is based on the local density approximation of the density functional theory for the low-frequency limit of the complex nonlocal spin susceptibility of the inhomogeneous electron gas $\chi(\boldsymbol{r}, \boldsymbol{r}'; \omega)$ [11, 23–26]. That susceptibility can be written in the form of an integral equation:

$$\chi(\boldsymbol{\rho}, \boldsymbol{\rho}' + \boldsymbol{R}_\alpha; \omega) = \chi_{\mathrm{P}}(\boldsymbol{\rho}, \boldsymbol{\rho}' + \boldsymbol{R}_\alpha; \omega) + \sum_{\beta=1}^{N} \int_{\mathrm{cell}} \chi_{\mathrm{P}}(\boldsymbol{\rho}, \boldsymbol{\rho}_1 + \boldsymbol{R}_\beta; \omega) \nu(n(\boldsymbol{\rho}_1 + \boldsymbol{R}_\beta)) \chi(\boldsymbol{\rho}_1 + \boldsymbol{R}_\beta, \boldsymbol{\rho}' + \boldsymbol{R}_\alpha; \omega)\, \mathrm{d}\boldsymbol{\rho}_1, \quad (1)$$

where $\nu(n(\boldsymbol{r}))$ is related to a second derivative of the exchange–correlation energy, and is (in the local-density approximation) a function only of the charge density n at $\boldsymbol{r}$. The quantity $\chi_{\mathrm{P}}(\boldsymbol{\rho}, \boldsymbol{\rho}' + \boldsymbol{R}_\alpha; \omega)$ is the 'noninteracting' Pauli susceptibility. The vectors $\boldsymbol{\rho}'$ and $\boldsymbol{\rho}_1$ are in the unit cell at the origin, and $\boldsymbol{R}_\alpha$ and $\boldsymbol{R}_\beta$ are lattice vectors. N is the number of unit cells.

The dependence of χ on N lattice vectors in real space can be replaced by a dependence on N vectors $\boldsymbol{q}_\alpha$ in the reciprocal lattice through the Bloch Fourier transform:

$$\tilde{\chi}(\boldsymbol{\rho}, \boldsymbol{\rho}'; \boldsymbol{q}_\alpha; \omega) = \sum_{\beta=1}^{N} \exp(\mathrm{i}\boldsymbol{q}_\alpha \cdot \boldsymbol{R}_\beta) \chi(\boldsymbol{\rho}, \boldsymbol{\rho}' + \boldsymbol{R}_\beta; \omega). \quad (2)$$

The $\nu(n(\boldsymbol{r}))$ that appears in equation (1) creates simultaneously the Stoner enhancement of the susceptibility, the core-polarization hyperfine fields, and the disenhancement factor in the spin–lattice relaxation rate [22]. Here we are mainly interested in the general expression for the relaxation rate:

$$S(T_1T)^{-1} = \frac{\mu_0}{4\pi} \left(\frac{4\mu_{\mathrm{B}}}{3} \right)^2 \frac{2}{N} \sum_{\alpha=1}^{N} \frac{\tilde{\chi}''(\boldsymbol{\rho}, \boldsymbol{\rho}; \boldsymbol{q}_\alpha; \omega_S - \omega_I)}{\hbar(\omega_S - \omega_I)}, \quad (3)$$

where $S = (2\mu_{\mathrm{B}})^2/(4\pi\hbar k\gamma^2)$, and ω_S and ω_I are the electronic and nuclear Larmor frequencies. The imaginary part of the susceptibility χ'' is an odd function of frequency, and linear for small values of ω. The right-hand side of equation (3) is then frequency independent

and can be evaluated in the limit of vanishing frequencies. The position in the unit cell of the nucleus under consideration is given by the vector $\boldsymbol{\rho}$.

Starting from equation (1), the static susceptibility, the Knight shift, and the relaxation rate for transition metals can be decomposed approximately into sums of s- and d-like contributions [22, 27], to which an additional orbital term [28] must be added:

$$\chi = \mu_0 \mu_B^2 \Omega^{-1} \left(\frac{D_s(E_f)}{1-\alpha_s} + \frac{D_d(E_f)}{1-\alpha_d} \right) + \chi_{orb} = \chi_s + \chi_d + \chi_{orb} \tag{4}$$

$$K = \frac{\Omega}{\mu_0 \mu_B} (\chi_s B_{hf,s} + \chi_d B_{hf,d} + \chi_{orb} B_{hf,orb}) = K_s + K_d + K_{orb} \tag{5}$$

$$S(T_1T)^{-1} = k_s K_s^2 + k_d K_d^2 R_d + (\mu_B D_d B_{hf,orb})^2 R_{orb}, \tag{6}$$

where Ω is the atomic volume; D_s and D_d are densities of states at the Fermi energy E_f; α_s and α_d are Stoner enhancement factors; the B_{hf} are effective hyperfine fields (including core polarization); k_s and k_d are Moriya disenhancement factors; and R_d and R_{orb} are reduction factors related to the decomposition of D_d into contributions of different symmetries $D_{t_{2g}}$ and D_{t_e}. The three densities of states $D_s(E_f)$, $D_{t_{2g}}(E_f)$ and $D_{e_g}(E_f)$ can be found from band-structure calculations, and the d-like hyperfine field can sometimes be determined by experiment. The $\alpha_l (l = s, d)$ are treated as fittable parameters. It is usually assumed that k_l can be calculated from some l-independent function of the Stoner parameter $k(\alpha)$; thus $k_l = k(\alpha_l)$. We have often used the Shaw–Warren result [29], that can be fitted to

$$k_{WS}(\alpha) = (1-\alpha)(1+\tfrac{1}{4}\alpha), \tag{7}$$

while the $k(\alpha)$ relation of the original Moriya equation [30, 31] can be approximately represented as

$$k_M(\alpha) = (1-\alpha)(1+\tfrac{5}{3}\alpha^2). \tag{8}$$

For strongly enhanced paramagnets, K and/or T_1T may become temperature dependent through spin fluctuations. Below, we summarize how these temperature dependences are expected to differ for ferromagnetic and antiferromagnetic enhancements. These theories have been developed for the homogeneous electron gas [32, ch 5], and we will give the relevant quantities an index h.

2.1. Paramagnets with ferromagnetic spin fluctuations

These are systems that show a strong temperature dependence of the uniform static susceptibility, but that nevertheless remain paramagnetic. The paramagnetic phase of low-T_C ferromagnets can be described by the same theory. In addition to an exchange parameter ν_h, spin fluctuation theory introduces a function $\delta(T)$, such that the temperature-dependent susceptibilities in a ferromagnetically enhanced paramagnet are given by

$$\tilde{\chi}_h(\boldsymbol{q}, T) = \frac{1}{\nu_h} \frac{\tilde{\chi}_{P,h}(\boldsymbol{q})}{(\delta(T)+1)\tilde{\chi}_{P,h}(\boldsymbol{0}) - \tilde{\chi}_{P,h}(\boldsymbol{q})}. \tag{9}$$

The Stoner enhancement factor is related to the exchange parameter and the $\boldsymbol{q} = \boldsymbol{0}$ static susceptibility through

$$\alpha_h = \nu_h \tilde{\chi}'_{P,h}(\boldsymbol{0}; \omega = 0) \tag{10}$$

and to the low-temperature limit of $\delta(T)$ by

$$\lim_{T \to 0} \delta(T) = \frac{1-\alpha_h}{\alpha_h}. \tag{11}$$

The inverse of the static uniform susceptibility, as in equation (4), is

$$\chi_{\mathrm{h}}^{-1}(T) = \Omega^{-1}\nu_{\mathrm{h}}\delta(T). \tag{12}$$

At low temperatures the usual Stoner-enhanced susceptibility is retrieved because of equation (11). At higher temperatures the usual Curie–Weiss behaviour implies that

$$\delta(T) \propto T - T_{\mathrm{C}} \tag{13}$$

and the cases of interest to us are close to the limit $T_{\mathrm{C}} \to 0$.

According to equation (12) the Knight shift becomes temperature dependent, and from equations (3) and (9) the spin–lattice relaxation rate is given by equation (14*a*) below:

$$S(T_1T)_{\mathrm{h}}^{-1} = \frac{2(\Omega B_{\mathrm{hf}})^2}{\pi\mu_0}\frac{\Omega}{(2\pi)^3}\int \frac{\tilde{\chi}''_{\mathrm{P,h}}(\boldsymbol{q};\omega)}{\hbar\omega}\frac{\delta(T)+1}{\alpha_{\mathrm{h}}}\left(\frac{1}{\delta(T)+1-F(\boldsymbol{q})}\right)^2 \mathrm{d}\boldsymbol{q} \tag{14a}$$

$$\approx S(T_1T)_{\mathrm{P,h}}^{-1}\frac{\delta(T)+1}{\alpha_{\mathrm{h}}}\left\langle\frac{1}{\delta(T)+1-F(\boldsymbol{q})}\right\rangle_{\mathrm{FS}}^2 \tag{14b}$$

$$\approx S(T_1T)_{\mathrm{P,h}}^{-1}\left(1+\tfrac{5}{3}(\delta(T)+1)^{-2}\right)\chi_{\mathrm{h}}(T)/\chi_{\mathrm{P,h}}, \tag{14c}$$

where $F(\boldsymbol{q})$ is the Lindhard function. The angular brackets in equation (14*b*) indicate an average over vectors $\boldsymbol{q}$ that connect two points on the spherical Fermi surface. The expression within large parentheses in equation (14*c*) comes from the approximation in equation (8). It is usually assumed that the main temperature dependence of T_1T is contained in the factor $\chi_{\mathrm{h}}(T)$, which for an incipient ferromagnet is $\propto 1/T$. The result is a T_1 independent of temperature, and a Knight shift $K \propto \chi_{\mathrm{h}}(T) \propto 1/T$. The low-temperature limit of equation (11) introduces the Moriya disenhancement factor of equation (8) into (14*c*):

$$(T_1T)_{\mathrm{h}}^{-1} = (T_1T)_{\mathrm{P,h}}^{-1}k_{\mathrm{M}}(\alpha_{\mathrm{h}}). \tag{14d}$$

2.2. Paramagnets with antiferromagnetic spin fluctuations

In antiferromagnetic systems, the static paramagnetic susceptibility has its maximum at an ordering vector $\boldsymbol{Q} \neq \boldsymbol{0}$. A moderate tendency towards antiferromagnetism has been found in calculations for bulk rhodium, where a secondary maximum in $\tilde{\chi}(\boldsymbol{q})$ appears at a nonzero wavevector [20], the absolute maximum remaining at $\boldsymbol{q} = \boldsymbol{0}$. In the NMR of the paramagnetic state of antiferromagnets a situation can arise where T_1 is dominated by $\tilde{\chi}''(\boldsymbol{Q})$, whereas the Knight shift is determined by $\tilde{\chi}'(\boldsymbol{0})$. In that case, there exists no equivalent of the $k(\alpha)$ relation as in equations (7) or (8), since the α in K refers to $\boldsymbol{q} = \boldsymbol{0}$, and that in T_1 to $\boldsymbol{Q}$.

There is no closed expression, analogous to equation (14*a*), for the spin–lattice relaxation in antiferromagnetically enhanced paramagnets. Still the temperature dependence of T_1T can be estimated in the following way. The starting assumption is that, because of the enhancement, $\tilde{\chi}''$ is strongest around a wavevector $\boldsymbol{Q}$ different from zero, and that around that wavevector it can be expanded as

$$\frac{\tilde{\chi}''(\boldsymbol{Q}+\boldsymbol{q};\omega)}{\hbar\omega} = \frac{C'}{\nu_Q(\delta_Q(T)+A'q^2)^2}, \tag{15}$$

where C' and A' are coefficients of the expansion, and ν_Q and $\delta_Q(T)$ are analogous to the quantities in ferromagnetic fluctuations theory. The sum in equation (3) is converted into an integral over a spherical volume equivalent to a Brillouin zone centred at $\boldsymbol{Q}$, of radius q_{B} such that $q_{\mathrm{B}}^3 = 6\pi^2/\Omega$, so $(T_1T)^{-1}$ is proportional to

$$\int_{q=0}^{q_{\mathrm{B}}} \frac{4\pi q^2}{\nu_Q(\delta_Q(T)+A'q^2)^2}\,\mathrm{d}q = \begin{cases} \dfrac{\pi^2}{A'\nu_Q\sqrt{A'\delta_Q(T)}} & \text{for } \delta_Q \to 0 \\ 2\pi q_{\mathrm{B}}^3\nu_Q\tilde{\chi}_P'^2(\boldsymbol{Q}) & \text{for } \nu_Q \to 0. \end{cases} \tag{16}$$

In the weak-enhancement limit, $\nu_Q \to 0$, T_1T is independent of T, as expected. In the limit of a strong antiferromagnet, $\delta_Q \to 0$, we have

$$T_1T \propto \sqrt{\delta(T)} \propto \sqrt{T - T_N} \tag{17}$$

and for an incipient antiferromagnet, $T_N \to 0$, the resulting relaxation rate is proportional to the square root of temperature.

The detection of antiferromagnetic enhancement by means of NMR is usually based on qualitative arguments. At low temperature the Knight shift is temperature independent, whereas T_1T is not. The experimental relaxation rate $T_1^{-1}(T)$ is fitted to

$$T_1^{-1} = aT + bT^{1/2}. \tag{18}$$

The term $\propto T$ is attributed to the term $\propto B_{\mathrm{hf,orb}}$ in equation (6). It is usually impossible to give a quantitative interpretation of the value of the parameter b. A recent example of antiferromagnetic spin fluctuations seen by means of NMR is provided by the ^{59}Co in $Zr_2(Co_{1-x}Ni_x)$ compounds [33].

3. Experimental details

We have studied four samples of small Rh particles using NMR. A first sample, denoted Rh/TiO_2, is one that was used previously [34] (average diameter 3.6 nm, dispersion 26%). A second one, Rh/PVP, has been prepared by the method described earlier [34], but with double the metal loading (i.e. 20% by weight) of the sample in that reference. The size distribution determined from transmission electron microscopy (TEM) is very similar (average diameter 3.0 nm, dispersion 37%) to that of the earlier sample, and the NMR spectra are indistinguishable. Two further samples were prepared by an impregnation method similar to that used for Rh/TiO_2, except that two different aluminas were used as carriers. A sample containing 20% by weight of Rh was prepared on RP3 alumina (Rhône-Poulenc). Its average diameter, as determined from TEM, is 2.6 nm, and the dispersion calculated from the size histogram is 40%. From a hydrogen adsorption isotherm at 318 K and assuming a 1:1 stoichiometry, its dispersion was found as 35%. The other sample was prepared on GSF400 alumina (Rhône-Poulenc) and has 4% loading. Its size distribution is difficult to measure by TEM; we have used small-angle x-ray scattering to estimate the average diameter as 1.5 nm and the dispersion as 54%. The approximate number of atoms in particles with the average diameter is 1800 for Rh/TiO_2, 1000 for Rh/PVP, 670 for Rh/RP3, and 130 for Rh/GSF400.

The NMR equipment was very similar to that described before [34], its main feature being a 14 T magnet with an incorporated sample cryostat (Oxford Instruments).

4. Results and discussion

4.1. NMR of bulk Rh compared to Pd

Bulk rhodium has the same fcc structure as palladium, its neighbour in the periodic system, and roughly the same density of states (DOS) curve, but a lower $D(E_f)$ and a moderate Stoner enhancement [11, 15]. While between 150 and 1500 K the bulk susceptibility of Pd decreases according to a Curie–Weiss law, the susceptibility of Rh increases monotonically with T from the lowest temperatures studied up to at least 1500 K [35]. The increase is of the order of half the average value. For comparison, the s-spin susceptibility of silver, the other neighbour of palladium, increases by something like 1/15 of the average value between 10 [36] and 1360 K [37], as measured from the ^{109}Ag NMR shift.

Table 1. Fitted values of partial contributions to the susceptibility, the Knight shift, and the relaxation rate of ^{103}Rh in rhodium metal. The next four rows give the parameters used: hyperfine fields $B_{\rm hf}$, reduction factors R, exchange integrals I, and densities of states $D(E_{\rm f})$. The molar volume $V_m = 8.30$ cm^3. For $\chi_{\rm cgs}$ in μemu mol^{-1}, multiply the table body entries by $V_m/(4\pi)$.

	s	d	Orb	Dia	Sum	Experiment
χ (10^{-6})	2.5	130.6	71.2	−59.7	144.6	143.8
K (10^{-3})	0.60	−5.25	8.42		3.76	3.75
$(T_1T)^{-1}$ (10^{-3} s^{-1} K^{-1})	1.3	11.6	96.9		109.8	111.5
$B_{\rm hf}$ (T)	200	−34	100			
R		0.20	0.44			
I (mRyd)	0	28				
$D(E_{\rm f})$ (Ryd^{-1})	0.7	18.0			18.7	

For both ^{105}Pd [38] and ^{103}Rh [39] the Knight shift data up to room temperature track the susceptibility. For ^{105}Pd this proportionality has been used to determine $B_{\rm hf,d}$, but for ^{103}Rh it has been argued [39, 40] that it cannot be the $\chi_{\rm d}$ alone that varies with temperature, because that would imply an unusually small d-like hyperfine field. Between 150 K and room temperature the T_1T for ^{105}Pd decreases slightly and this variation has been fitted to a spin fluctuation expression [41] similar to equation (14*c*). The relaxation data for ^{103}Rh have not been analysed in comparable detail.

The Knight shift of bulk Rh is nearly temperature independent up to 100 K and then decreases (becomes less positive) going to room temperature. We find the metal resonance at low temperatures at 1.343 73(5) MHz T^{-1}, in excellent agreement with the literature value of 1.343 74(3) MHz T^{-1} [40]. But because we use another reference frequency [3], we give the corresponding Knight shift as $K = 3.75 \times 10^{-3}$, instead of 4.3×10^{-3}. At 280 K, we have $K = 3.57 \times 10^{-3}$. Between 15 and 200 K, we find the relaxation rate linear in temperature, with $T_1T = 8.97(5)$ s K, in agreement with the earlier result 9 s K at helium temperatures [40].

These low-temperature NMR data for bulk Rh can be fitted by the usual equations (4)–(7); see table 1. In this fit, the diamagnetic susceptibility of Rh was set equal to that of Ag (-39.4 μemu mol^{-1} in cgs units), as calculated from the total experimental susceptibility of silver (-19.5 μemu mol^{-1}) and its spin susceptibility as determined from ^{109}Ag NMR [3] (19.9 μemu mol^{-1}). The reduction factors R were set to equal occupancy for all five types of d orbital, and a term 1/25 was added to $R_{\rm orb}$ to account for dipolar relaxation [28]. Since $D_{\rm s}(E_{\rm f})$ is low anyway, the corresponding exchange integral $I_{\rm s} = \alpha_{\rm s}/D_{\rm s}(E_{\rm f})$ was set to zero; for the same reason the s-like hyperfine field was simply set to a plausible value, the fitted value for Pd [3]. The d-like hyperfine field was constrained to be between zero and the value determined experimentally for Pd [38]. The orbital susceptibility and hyperfine field were constrained to be comparable to calculated values [42]. The d-like exchange integral $I_{\rm d}$ was constrained to yield a moderate susceptibility enhancement. The fitted enhancement factor is 2.02, in reasonable agreement with a calculated value of 1.79 [11]. The parameter values obtained here are somewhat different from those in the preliminary analysis proposed in [34]. The latter unfortunately contains numerical errors and is therefore inconsistent.

4.2. ^{103}Rh spectra of small rhodium particles

The ^{103}Rh spectra for the four small-particle samples are shown in figure 1. In principle, nuclei in noncubic sites (e.g. in the surface) have anisotropic Knight shifts, that give rise to powder lineshapes with characteristic shoulders [43]. Such features do not show up here, presumably because the site-to-site variation of the shift is larger than the difference in shift

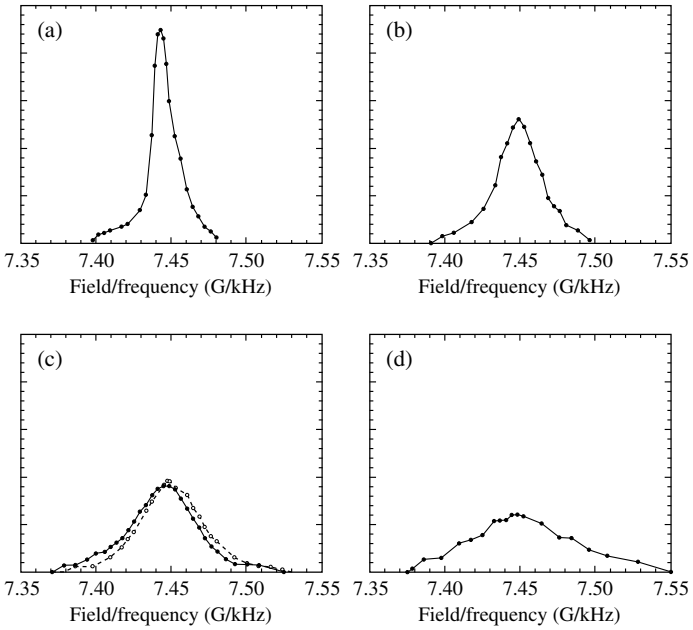

Figure 1. Point-by-point ^{103}Rh NMR spectra for clean-surface Rh particles of different sizes on different supports, taken at 80 K. The spectra are normalized to the same area. The samples are (a) Rh/TiO_2, (b) Rh/PVP, (c) Rh/RP3, (d) Rh/GSF400. The dotted curve in (c) shows the effect of chemisorption of a monolayer of hydrogen. On this scale, the width of the bulk Rh resonance is comparable to the line thickness.

tensor elements on a single site. All spectra in figure 1 are approximately centred at the bulk resonance position, and broaden rather symmetrically when the particle size decreases. Chemisorption of hydrogen has a measurable, but rather small effect; figure 1(c). These spectral characteristics are markedly different from those of small platinum particles [9, 44], where the intensity in the ^{195}Pt spectra shifts from the bulk resonance position to zero Knight shift (the 'surface resonance' position) when the particle size diminishes and where the spectral shape changes qualitatively when hydrogen is adsorbed.

There are two reasons for this different behaviour: one related to the NMR of Rh metal, the other related to the electronic structure of the Rh surface. According to table 1, the Knight shift and the relaxation rate of bulk Rh are dominated by the orbital parts, with additional contributions from the spins of the d-like electrons, and negligible s-like parts. This is very different from the cases for Pt or Pd, where the d-like spin part dominates, and the orbital parts are nearly negligible [3]. For small particles of Pt (and presumably also of Pd), the magnetic behaviour can be reasonably well described by considering only the site-to-site variation of the d-like spin part, and as it happens this part of the susceptibility is measurably smaller on surface sites than in the bulk. For that reason, a 'layer model' [9, 45] is successful for Pt (and probably would also be for Pd, if the experiment could be done). From calculations for a rhodium slab [16] the site-to-site variation of the ^{103}Rh (spin) Knight shift is expected to be comparatively small: therefore the spectral shapes in figure 1 are probably dominated by competition between (positive) orbital shifts and (negative) spin shifts. On some surface sites the net result is negative, on others positive; therefore no clear surface signal can be found in the spectra. From calculations for the fcc(111) surfaces for Pd and Rh [14] it is found that

hydrogen has markedly less influence on $D(E_f)$ at surface sites on rhodium than on palladium. It is believed that in this respect Pt behaves as Pd, which would explain why the ^{195}Pt spectral shape shows large qualitative changes upon hydrogen adsorption, whereas the ^{103}Rh spectrum in figure 1(c) only shows a small shift (by about 14 kHz or 740 ppm, to higher field).

4.3. Spin–lattice relaxation of ^{103}Rh in small particles

In ^{195}Pt NMR of clean-surface particles the relaxation rate at a given resonance position is independent of support or particle size [8] (with the exception of zeolite carriers). Therefore Pt nuclei in different samples that resonate at the same spectral position are in very similar environments. Such a simple identification of atomic environment with spectral position cannot be made for Rh particles: at the same resonance position, we can find very different relaxation rates.

In the sample with the largest particles, Rh/TiO_2, the value of T_1T is roughly the same at 80 and 20 K for several spectral positions; see figures 2(a), (b). Assume for the sake of argument that the full line in figure 2(b) correctly represents the spectral variation of the product T_1T. It is nowhere larger than the bulk value and, the contribution of $D_s(E_f)$ to the relaxation being negligible, equation (6) indicates that there can be no atomic sites with a LDOS $D_d(E_f)$ smaller than the bulk value. The symmetry of the NMR spectrum and of the sketched T_1T curve imply that there must also be a site-to-site variation of the orbital susceptibility χ_{orb}. The parts (c) and (d) of figure 2 show the relative changes across the spectrum of $D_d(E_f)$ and χ_{orb}, assuming all other parameters in table 1 to be constant.

At the low-field end of the spectrum for somewhat smaller particles, Rh/PVP, the relaxation rate is less than it is in the bulk; see figures 3(a), (b). Since the orbital relaxation rate should be unaffected by magnetic fluctuations, this immediately says that at least in part of this sample, the LDOS is lower than $D(E_f)_{bulk}$. There is a clear low-temperature enhancement of the relaxation rate over most of the spectral width, while the spectral shape in figure 3(a) hardly varies.

For still smaller particles, the spectral shape remains nearly independent of temperature, but the products T_1T vary strongly; see figures 3(c), (d). At fixed temperature, the site-to-site variation of the relaxation is relatively small, since T_1 is nearly constant across the spectrum. From the lines drawn in figure 3(d) we have at the bulk resonance position $T_1^2T = 0.63 \pm 0.03$ s^2 K for the two temperatures. This is a strong indication of relaxation dominated by the term $bT^{1/2}$ in equation (18). The relative unimportance of the term aT implies a drop in $D(E_f)$ with respect to the bulk value, as has already been seen at the low-field end in figure 3. Since the spectrum remains centred at the bulk position, there must be a drop in χ_{orb} as well.

The smallest particle sample in figure 1(d) has a low loading and a large spectral width, which makes it very difficult to perform the relaxation measurements. Some results (not shown) have been obtained at 80 K. Their large error bars range from the 80 K values in figure 3(b) to those in figure 3(d). Very qualitatively the results agree with those for the other samples, but the large error range and the lack of low-temperature data prevent further discussion.

5. Conclusions

The ^{103}Rh NMR of the 3.6 nm particles, Rh/TiO_2, is mainly determined by surface effects. Calculations for slabs exhibiting different Rh surfaces [15, 16] indeed show enhanced values of $D(E_f)$ at the surface, as suggested by the curve in figure 2(c). From comparison with figure 2(d), it follows that on sites where $D_d(E_f)$ increases, χ_{orb} increases also.

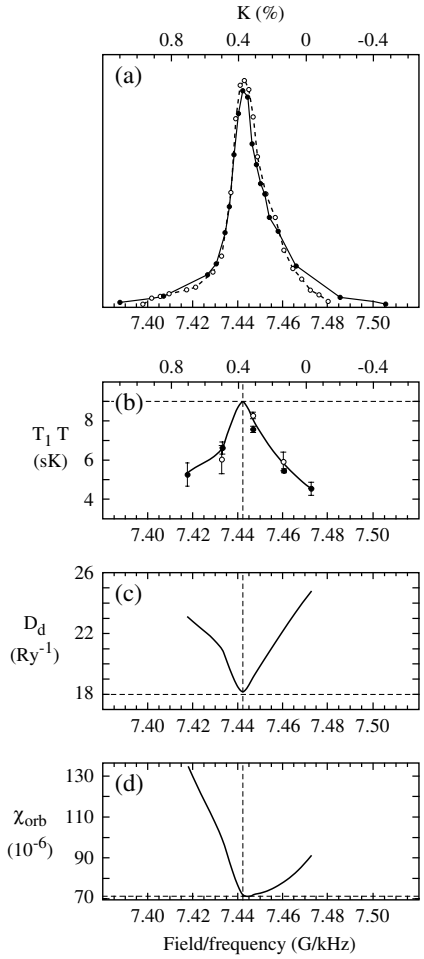

Figure 2. The NMR spectrum (a) and value of T_1T for several spectral positions (b) in sample Rh/TiO_2, at 20 (full circles) and 80 K (open circles). The line drawn in (b) is meant to suggest that T_1T is independent of temperature, and that it is close to the bulk value (straight dashed lines) in the centre of the spectrum. The line drawn in (b) can be represented by the variations of $D_d(E_f)$ and of χ_{orb} shown in (c) and (d).

In particles of 3.0 nm, Rh/PVP, the T_1-values at 80 K show that at least in a part of the sample $D_d(E_f)$ is less than the bulk value. The spectrum stays symmetric and centred at K_{bulk}, which suggests that where $D_d(E_f)$ diminishes, χ_{orb} diminishes also. We believe that this is a size effect rather than a surface effect, that somehow accompanies the onset of the size-dependent antiferromagnetic relaxation enhancement. This enhancement is more clearly seen at 20 K; at 80 K it is decreased by spin fluctuations. For the particles in this sample the enhancement is probably in between the two limits of equation (16), so the overall temperature dependence of T_1T does not have the structure of equation (18).

The very similar values of T_1^2T at the two temperatures for the bulk resonance position in figure 3(d) suggest that here equation (18) might be applicable. However, the considerable amount of experimental time that would be required has kept us from gathering enough data to do a $T_1^{-1} = aT + b(T - T_N)^{1/2}$ analysis, for which an interpretation of a and b would be

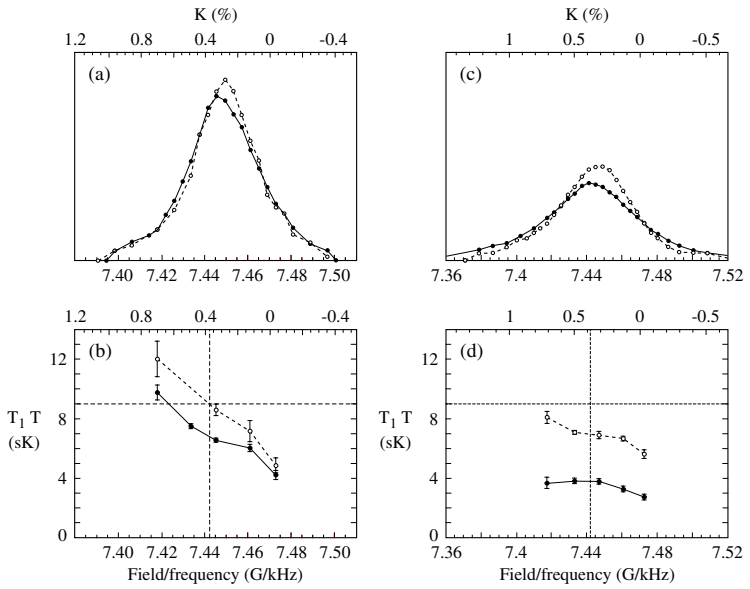

Figure 3. The NMR spectrum (a) and value of T_1T for several spectral positions (b) in sample Rh/PVP, at 20 (full circles) and 80 K (open circles). The lines in (b) are drawn only to connect points at the same temperature. The temperature effect on the relaxation (but not on the spectrum) is much larger than in figure 2. At the low-field end in (b) the relaxation is slower than in bulk Rh (straight dashed lines). Similar data for sample Rh/RP3 are shown in (c) and (d). Here the site-to-site variation is rather small, but the temperature effect is large.

difficult anyway. To illustrate this point, assume that in figure 3(d) the a-term has half the value of the bulk relaxation, $\approx 0.05\ \mathrm{s}^{-1}\ \mathrm{K}^{-1}$, and furthermore that we are in the $\delta_Q \to 0$ limit of equation (16). In that case, our two temperature points could be fitted by assuming $T_N \approx 5$–10 K, and $\chi_{orb} \approx 0.7\chi_{orb,bulk}$.

The only modest variation of T_1 across the spectrum in figure 3(d) suggests that the relaxation mechanism acts more or less in the same way on all atomic sites: it is related to a size effect rather than a surface effect. Magnetism has been found in Rh clusters of up to $\approx$80 atoms, both experimentally [18] and theoretically [15]. Our particles in Rh/PVP and Rh/RP3 are larger (at least several hundreds of atoms), but the tendency towards magnetism now expresses itself through an enhancement of the antiferromagnetic $\tilde{\chi}(\boldsymbol{Q})$ found in calculations for the bulk [20]. A simple extrapolation of $T_1^2T = 0.63\ \mathrm{s}^2\ \mathrm{K}$ found from figure 3(d) towards higher temperatures says that the spin fluctuations will decrease the spin–lattice relaxation rate to below the bulk value for temperatures above 120 K. But in principle the antiferromagnetic character is already present at the unenhanced Pauli level [20] of $\chi_P(\boldsymbol{q})$, and it should not disappear on increasing the temperature. It is therefore not necessary that any of the NMR characteristics of the large-particle sample can be retrieved by increasing the temperature of the small-particle sample.

In summary, we have presented evidence from ^{103}Rh NMR that rhodium particles of approximately 2.6 nm diameter show incipient antiferromagnetism below 80 K. We suggest that this finding is related to the calculated [20] wavevector dependence of $\tilde{\chi}(\boldsymbol{q})$ for the bulk, and to the magnetism found in Rh clusters of less than 80 atoms, both in experiments [18] and in calculations [15]. The incipient antiferromagnetism is accompanied by a lowering of the density of states at the Fermi level and of the orbital susceptibility with respect to their bulk values.

Acknowledgments

This work was supported by the Swiss National Science Foundation under grant 20-53637.98. We thank Albert Renouprez and members of his group at the Institut de Catalyse, Lyon; Danièle Laub at the CIME of the EPFL, and Janet Kesselman, then at the ICP/EPFL, for their practical help with several aspects of this work, as well as for illuminating discussions.

References

[1] Dreyssé H and Demangeat C 1997 *Surf. Sci. Rep.* **28** 65
[2] Bucher J P and Bloomfield L A 1993 *Int. J. Mod. Phys.* B **7** 1097
[3] van der Klink J J and Brom H B 2000 *Prog. NMR Spectrosc.* **36** 89
[4] Kubo R 1962 *J. Phys. Soc. Japan* **17** 975
[5] Kobayashi S, Takahashi T and Sasaki W 1972 *J. Phys. Soc. Japan* **32** 1234
[6] Yee P and Knight W D 1975 *Phys. Rev.* B **11** 3261
[7] Stokes H T, Rhodes H E, Wang P K, Slichter C P and Sinfelt J H 1982 *Phys. Rev.* B **26** 3575
[8] van der Klink J J 2000 *Adv. Catal.* **44** 1
[9] Bucher J P, Buttet J, van der Klink J J and Graetzel M 1989 *Surf. Sci.* **214** 347
[10] Weinert M and Freeman A J 1983 *Phys. Rev.* B **28** 6262
[11] Janak J F 1977 *Phys. Rev.* B **16** 255
[12] Kirchner B, Weber W and Voitländer J 1994 *J. Phys.: Condens. Matter* **6** 2603
[13] Louie S G 1979 *Phys. Rev. Lett.* **42** 476
[14] Löber R and Hennig D 1997 *Phys. Rev.* B **55** 4761
[15] Barreteau C, Guirado-López R, Spanjaard D D, Desjonquères M C and Olés A M 2000 *Phys. Rev.* B **61** 7781
[16] Eichler A, Hafner J, Furthmüller J and Kresse G 1996 *Surf. Sci.* **346** 300
[17] Goldoni A, Baraldi A, Barnaba M, Comelli G, Lizzit S and Paolucci G 2000 *Surf. Sci.* **454–6** 925
[18] Cox A J, Louderback J G, Apsel S E and Bloomfield L A 1994 *Phys. Rev.* B **49** 12 295
[19] Winter H, Stenzel E, Szotek Z and Temmerman W M 1988 *J. Phys. F: Met. Phys.* **18** 485
[20] Sandratskii L M and Kübler J 1992 *J. Phys.: Condens. Matter* **4** 6927
[21] Staunton J B, Poulter J, Ginatempo B, Bruno E and Johnson D D 2000 *Phys. Rev.* B **62** 1075
[22] van der Klink J J 1996 *J. Phys.: Condens. Matter* **8** 1845
[23] Vosko S H and Perdew J P 1975 *Can. J. Phys.* **53** 1385
[24] Gunnarson O 1976 *J. Phys. F: Met. Phys.* **6** 587
[25] Williams A R and von Barth U 1983 in [26]
[26] Lundqvist S and March N H 1983 *Theory of the Inhomogeneous Electron Gas* (New York: Plenum)
[27] Yafet Y and Jaccarino V 1964 *Phys. Rev.* A **133** 1630
[28] Obata Y 1963 *J. Phys. Soc. Japan* **18** 1020
[29] Shaw R W and Warren W W 1971 *Phys. Rev.* B **3** 1562
[30] Moriya T 1963 *J. Phys. Soc. Japan* **18** 516
[31] Narath A and Weaver H T 1968 *Phys. Rev.* **175** 373
[32] Moriya T 1985 *Spin Fluctuations in Itinerant Electron Magnetism* (Berlin: Springer)
[33] Takekuni M, Sugita H and Wada S 1998 *Phys. Rev.* B **58** 11 698
[34] Vuissoz P A, Yonezawa T, Yang D, Kiwi J and van der Klink J J 1997 *Chem. Phys. Lett.* **264** 366
[35] Abart J, Sänger W and Voitländer J 1982 *J. Magn. Magn. Mater.* **28** 282
[36] Bercier J J 1993 *Thesis* EPFL, Lausanne
[37] El-Hanany U, Shaham M and Zamir D 1974 *Phys. Rev.* B **10** 2343
[38] Seitchik J A, Gossard A C and Jaccarino V 1964 *Phys. Rev.* **136** A1119
[39] Seitchik J A, Jaccarino V and Wernick J H 1965 *Phys. Rev.* **138** A148
[40] Narath A and Weaver H T 1971 *Phys. Rev.* B **3** 616
[41] Takigawa M and Yasuoka H 1982 *J. Phys. Soc. Japan* **51** 787
[42] Ebert H, Battocletti M, Deng M, Freyer H and Voitländer J 1999 *J. Comput. Chem.* **20** 1246
[43] Bloembergen N and Rowland T J 1953 *Acta Metall.* **1** 731
[44] Rhodes H E, Wang P K, Stokes H T, Slichter C P and Sinfelt J H 1982 *Phys. Rev.* B **26** 3559
[45] Makowka C D, Slichter C P and Sinfelt J H 1985 *Phys. Rev.* B **31** 5663